Longitudinal control for person-following robots

Citation for the original published paper (version of record):
Wang, L., Wu, J., Li, X. et al (2022). Longitudinal control for person-following robots. Journal of Intelligent and Connected Vehicles, 5(2): 88-98. http://dx.doi.org/10.1108/JICV-01-2022-0003

Longitudinal control for person-following robots

Liang Wang
China Academy of Transportation Sciences, Beijing, China
Jiaming Wu
Department of Architecture and Civil Engineering, Chalmers University of Technology, Gothenburg, Sweden
Xiaopeng Li
University of South Florida, Tampa, Florida, USA, and
Zhaohui Wu and Lin Zhu
China Academy of Transportation Sciences, Beijing, China

Abstract

Purpose – This paper aims to address the longitudinal control problem for person-following robots (PFRs) for the implementation of this technology.

Design/methodology/approach – Nine representative car-following models are analyzed from PFRs application and the linear model and optimal velocity model/full velocity difference model are qualified and selected in the PFR control.

Findings – A lab PFR with the bar-laser-perception device is developed and tested in the field, and the results indicate that the proposed models perform well in normal person-following scenarios.

Originality/value – This study fills a gap in the research on PRFs longitudinal control and provides a useful and practical reference on PFRs longitudinal control for the related research.

Keywords Person following robot, Longitudinal control model, Parameter optimization

Paper type Research paper

1. Introduction

Person-following scenarios arise when a lead human and an autonomous robot collaborate on a common task where the robot needs to follow the leading human's movements (Islam *et al.*, 2018). The basic function of a person-following robot (PFR) is to obtain the position of its leading person (LP) and to follow the LP continuously during executing a task. In recent years, the PFR technology has been applied in several domains, such as manufacturing, health care, entertainment industry and social interactions (Ren *et al.*, 2016; Islam, 2018; Cha and Chung, 2020).

Generally, a complete PFR includes two components, hardware and a control unit (Figure 1). The hardware of a PFR includes perception devices, robot chassis systems and energy systems. The perception device includes an LP position module and an environment perception module. The former provides the basic following function for a PFR. Stability and low latency are required for the LP position perception. The latter, the environment perception device, is designed for advanced functions of a PFR, including obstacle avoidance, gesture identification and route optimization. For some PFRs, the functions of obtaining LP position and environment are integrated into one perception device (Ren *et al.*, 2016; Cha and Chung, 2020; Bao *et al.*, 2017). The control unit is the essential part of a PFR, analyzing hardware data and controlling PFR's hardware. According to its function, control units can be categorized into the basic and complex following control units, as shown in Figure 1. The basic following control unit handles a PFR's following functions, including analyzing the data from the LP perception device and calculating a PFR's motion at the next calculation period. The basic following control unit functions as the cerebellum of a human and controls the basic functions of a PFR. Calculation speed, stability and low latency are critical to a basic following control unit. The complex following control unit manages the advanced functions of PFR, such as analyzing data from environment perception devices, obstacle avoidance, routing planning, gesture identification for interaction with the LP and

The current issue and full text archive of this journal is available on Emerald Insight at: **https://www.emerald.com/insight/2399-9802.htm**

Journal of Intelligent and Connected Vehicles
5/2 (2022) 88–98
Emerald Publishing Limited [ISSN 2399-9802]
[DOI 10.1108/JICV-01-2022-0003]

This work was supported by the Basal Research Fund of Central Public Research Institute of China (Grant No. 20212702).

Received 25 January 2022
Revised 27 February 2022
Accepted 28 February 2022

Figure 1 The structure of a person-following robot (PFR)

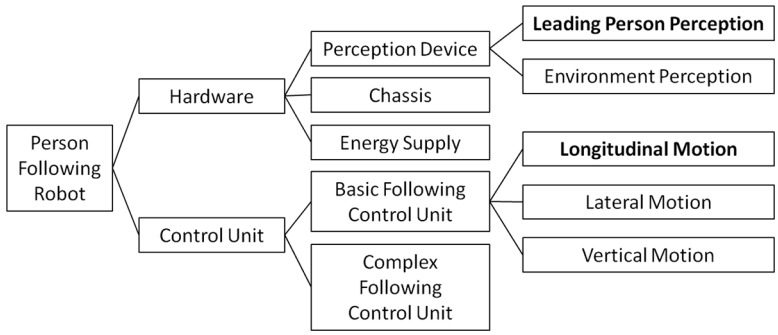

interaction with other PFRs in a team following scenario (Bae *et al.*, 2022; Austria *et al.*, 2021; Minaeian *et al.*, 2017). High computation power is desirable for complex tasks, such as image recognition and AI analysis.

The study of longitudinal control involves two main parts of a PFR, including leading person perception and longitudinal motion control (Figure 1). The data received from the perception device working on leading person perception is the input of the study and the PFR longitudinal motion is the output of this study.

Although many studies on the PFRs have been conducted in recent years, most of them focused on perception (Wu *et al.*, 2021a; Algabri and Choi, 2021) but overlooked controlling, especially following the LP longitudinally. The linear control strategy (Olatunji *et al.*, 2020; Satake and Miura, 2009; Le *et al.*, 2018) is proposed to control a PFR. The governing equation is a linear function of the gap for longitudinal control. If a camera is applied to obtain the LP's position, the gap between PFR and LP is noted by the number of the LP's pixels on the photosensitive sensors (Tarokh *et al.*, 2008). When the gap increases, the number of pixels of the LP decreases and the speed increases according to the control strategy. The fuzzy logic control strategy is proposed to compute the appropriate velocity for a PFR (Jia *et al.*, 2013). Based on the fuzzy logic, the gap between the LP and the PFR is divided into five segments, including "very far", "far", "safe distance", "close" and "very close" segments. Although the constants for each segment are different, the governing equations in the longitudinal direction are still linear functions of the gap. The decision tree is applied to control a PFR (Kautsar *et al.*, 2019; Ren *et al.*, 2016). The decision tree covers the basic motions of the PFR, including stopping, turning, reversing and moving forward. In the decision tree, the moving forward speed (noted by the controlling signal PWM) is a linear function of the gap between the LP and the PFR. The PID controller is introduced in the PFR longitudinal control (Tarokh and Kuo, 2008; Cheng *et al.*, 2019; Peralta *et al.*, 2018; Zhang *et al.*, 2019). To keep a re-specified distance during the following, the proportional and differential components of the PID controller are applied to control PFR's speed.

Generally, the studies on the PFR longitudinal control models are insufficient, rarely discussed independently. As a result, several longitudinal control exclusive research topics, including the LP's motion features, PFR's following stability and gap range are still deficient. The current control studies of the PFR are not enough to handle the high demands of the PFR including intense speed changes, stop-and-go, LP's periodic/random movement and reverse. As a result, reasonable and practical longitudinal control models for the PFR are required.

The contributions made in this paper can be summarized as follows: First, the challenges and exclusive features of PFR longitudinal control are summarized, including reverse, gap range, no imitation and the LP's periodic/random movement. Such challenges and features are the main goals or requirements for the following studies of PFR longitudinal control. Second, the knowledge of the car-following/automated driving control model is introduced into person-following studies after modification and parameter optimization. Such knowledge transferring can improve the PFR's longitudinal control study. Third, this study provides a comprehensive and quantifiable evaluation criterion for model and parameter optimization. Many key features are considered in the presented evaluation criterion, including motor capacity, perception devices' measurement range, energy-saving, gap range and LP's using feeling. Fourth, a lab PFR with the bar-laser-perception device is developed and tested in the field and the results indicate that the proposed models perform well in normal person-following scenarios.

The paper is organized as follows. Section 2 states the exclusive features of PFR longitudinal control; Section 3 revises nine representative car-following/autonomous driving models to select appropriated control models for PFRs. Section 4 presents the method of optimizing parameters of the selected optimization and numerical experiments for illustrating the application of the selected models are conducted. Finally, Section 5 introduces our bar-laser-perception device for PFR developed in-house and reports the field test results.

2. Different features between car-following and person-following

A car-following model describes and simulates the driver's longitudinal reaction during following a leading vehicle in the same lane. Replacing the leading vehicle with an LP and replacing the following vehicle with a PFR, a car-following scenario is similar to a person-following scenario. The similarity stands out especially considering the recent development of connected and automated vehicles (Li and Li, 2019; Wu *et al.*, 2020, 2021a, 2021b). Thus, it is reasonable to introduce the knowledge of car-following into a person-following scenario. However, to successfully transfer the knowledge into the PFR

control context, the differences between car-following and person-following need to be addressed. In this section, several exclusive features of person-following are listed.

2.1 Reverse

Car-following models are meant to describe forward vehicle dynamics in highway traffic, while they usually do not consider reverse movements. However, for a PFR, reverse within a small distance at a slow speed may be needed at times. Two typical situations required reverse for a PFR. First, when controlling a PFR in a narrow indoor space where a U-turn is infeasible, reverse movements at a slow speed are ineluctable. Second, the LP may not always stay at a non-negative velocity as vehicles do and instead, the LP may move slightly backward from time to time for maneuver convenience in certain tasks.

2.2 Gap range

The research of car-following considers the shortest following gap for driving safety but usually does not record the longest gap during operation. For example, if there is no leading vehicle ahead or the leading vehicle's speed is too higher to follow, the subject driver ignores his/her leading vehicle and gets into the free-drive state, which means the driver control speed by himself/herself desire. However, for a PFR, the values of shortest and longest gaps are all important for two reasons. First, common perception sensors used in PFRs are sensitive to distance. Once the following gap extends the measurement range of sensors during operation, the person following behavior is failed. Second, a PFR may lose its LP during following with a long gap (particularly at corners or in a crowded environment). A vehicle can drive without leading vehicles, but a PFR can't work without its LP. And it is a low probability that a PFR can restore after its LP is missing. Therefore, it is critical to keep a reasonable gap range during operations for PFRs.

2.3 No imitation

A car-following model is designed to imitate a driver's behavior on a highway. Some of the car-follow models were developed to explain observed highway traffic phenomena such as shock wave, traffic oscillation and capacity drop (*Zhu, 2001*). Even models for automated vehicle control are often designed to reproduce a good driver's control (Milanés and Shladover, 2014). Such imitation also includes a driver's limitation on observation and judgment. However, a PFR's movements are not necessarily confined by particular human behaviors. The only purpose of a PFR longitudinal model is to control the subject PFR to follow its LP reliably and smoothly.

2.4 Leading person's periodical and random movements

Human walking or running includes periodical movements caused by the alternate movements of the legs. When the LP stops for some reason, such as waiting for a traffic light, the LP is not as still as a stopped vehicle. Instead, the LP may have random movements in the longitudinal direction. The LP's periodical and random movements do not happen in a car-following scenario.

3. Model feasibility analysis

Car-following models have been studied for over half a century (Gazis *et al.*, 1959; Ahmed *et al.*, 2021; Brackstone and Mcdonald, 1999), and many types of models are well developed and wildly-used in traffic simulation and vehicle control. In this section, nine types of car-following/autonomous driving models are revised to select appropriated control models for PFRs based on the exclusive features of PFRs listed in Section 2.

3.1 Gazis Herman Rothery model

The GHR model was first introduced in the year 1958 and its formulation is:

$$a_n(t) = cv_n^m(t)\frac{\Delta v_n(t-\Delta t)}{\left(\Delta x_n(t-\Delta t)\right)^l} \tag{1}$$

here, $a_n(t)$ and $v_n(t)$ are the acceleration and speed of the subject vehicle (indexed by n) at time t; $\Delta x_n(s^2) := x_{n-1}(s^2) - x_n(s^2)$ and $\Delta v_n(s^2) := v_{n-1}(s^2) - v_n(s^2)$ are the following gap and the speed difference between the subject vehicle and its lead vehicle (indexed by $n-1$), respectively; Δt is the driver reaction time; m, l *and* c are the coefficients that may be calibrated with real-world data. The GHR model were configurated into different forms including General Motors model (Chandler and Montroll, 1958) with $m = 0$ and $l = 0$, Herman, Montroll, Potts and Rothery's model (Herman and Rothery, 1965) and Herman and Potts's model (Lasdon *et al.*, 1959) with $m = 0$ and $l = 1$, Treiterer and Myers's model (Treiterer and Myers, 1974) with $m = 0.7/0.2$ and $l = 2.5/1.6$. Ozaki's model (Ozaki, 1993) with $m = 0.9/-0.2$ and $l = 1/0.2$.

From equation (1), the subject vehicle's acceleration is proportional to a power term of its speed, the speed difference between the follower and the leader and a power term of the space headway. Note that equation (1) indicates that the control as required acceleration (the left-hand side) is zero if the speed difference $\Delta v_n(t-\Delta t)$ is zero regardless of the value of following gap $\Delta x_n(t-\Delta t)$. Thus, this control logic cannot easily maintain the following gap in the required gap range to a target value if the LP and the PFR are about at the same speed, which violates the feature specified in Section 2.2.

3.2 Psychophysical models

The first discussion of these models was given by Michaels (Michaels, 1963). The basic concept is that a car following is divided into several phases, and these phases are determined by some threshold values by the drivers (Wiedemann, 1974). Multiple phases are introduced to mimic a driver's decision process and the threshold values describe the perception limitation of humans. Although the psychophysical models are suitable to describe drivers' behavior of thinking and perception, such imitation of drivers' observation and analysis limitations is not necessary for PFRs. The psychophysical models violate the feature specified in Section 2.3.

3.3 Cellular automata model

The cellular automata model was first proposed by Nagel and Schreckenberg (1992). The model takes time and space as discrete variables, and a road lane is represented by many cells with equal sizes [typically 7.5-m long, according to Cha and Chung (2020)], which can either be empty or occupied by at

most one vehicle. The longitudinal movements of vehicles at each time step are described by implementing acceleration, braking, randomization and driving rules for all vehicles. The models are computationally efficient for large-scale simulation, yet they are not designed to capture detailed and precise microscopic movements due to the discretization of time and space. Thus, they are not suitable for microscopic control or PFRs over continuous time and space.

3.4 Collision avoidance model

In a collision avoidance model, the subject vehicle always maintains a safe distance from the leading vehicle and the subject vehicle will finally stop with a minimum acceptance gap to the leading vehicle when the leading vehicle brakes. The major development of the collision-avoidance model is made by Gipps (1981), and the widely used governing equation is:

$$v_n(t) = \min\{v_n(t-\Delta t) + 2.5a_n\Delta t\left[1 - v_n(t-\Delta t)/V_n\right]\left[0.025 + v_n(t-\Delta t)/V_n\right]^{1/2}, \\ b_n\Delta t + \sqrt{b_n{}^2\Delta t^2 - 2b_n\left[x_{n-1}(t-\Delta t) - l_{n-1} - x_n(t-\Delta t) - v_n(t-\Delta t)\Delta t\right] - b_n v_{n-1}^2(t-\Delta t)/\hat{b}}\} \tag{2}$$

where V_n is the desire speed for the subject vehicle, a_n is the acceleration of the subject vehicle, b_n is the maximum deceleration of the subject vehicle, $\hat{b}$ is the maximum deceleration of the leading vehicle based on the expectation of subject vehicle. The first part of equation (2) describes a free drive state and the second part illustrates the following state.

Note that the computation of the safety speed component in equation (2) assumes non-negative speeds for both the subject and lead vehicles (or otherwise, the square root term would not be well defined). Thus, the collision-avoidance model does not fit the PFR control that needs to accommodate occasional reverse movements. The collision avoidance model violates the feature specified in Section 2.1.

3.5 Linear models

Helly model (Helly, 1959) is a widely used linear model. A desire following gap from the lead vehicle is introduced in this model, and the subject vehicle tries to maintain the desire following gap. The governing equation is:

$$a_n(t) = C_1\Delta v_n(t-\Delta t) + C_2\left(\Delta x_n(t-\Delta t) - D_n(t)\right) \tag{3}$$

where $D_n(t)$ is defined as:

$$D_n(t) = D_0 + C_3 v_n(t) \tag{4}$$

where C_1,C_2,C_2 are constant coefficients. $D_n(t)$ is the desire following gap. D_0 is the desire following gap when speed is 0. It is convenient to control the following gap by adjusting the parameters of $D_n(t)$ directly. The concept of maintaining a target following gap is also applicable to the PFR longitudinal control.

We note that the linear model is suitable for the PFR control, as they accommodate reverse movements and have sufficient flexible parameters to be calibrated based on PFR applications.

3.6 Optimal velocity model

Bando *et al.* (1995) proposed an optimal velocity model (OVM) for car-following stimulation. The OVM is based on the idea that the subject vehicle desires to maintain an optimal velocity at any time, depending on the following gap from the leading vehicle. The driver tries to reduce the difference between the desired optimal velocity and its actual velocity in the car-following operation. Several key properties of real-world traffic flows can be described by OVM, such as the instability of traffic flow, the evolution of traffic congestion and the formation of stop-and-go waves (Jiang *et al.*, 2001). The governing equation is:

$$a_n(t) = \kappa\left[V\left(\Delta x_n(t-\Delta t)\right) - v_n(t-\Delta t)\right] \tag{5}$$

where κ is a sensitivity constant and $V(s^2)$ is the optimal velocity that the driver prefers. The optimal velocity function is:

$$V(\Delta x) = V_1 + V_2\tanh[C_1(\Delta x) - C_2] \tag{6}$$

where Δx is the gap between the subject vehicle and the leading vehicle; V_1,V_2,C_1,C_2 are constant parameters, which need to adjust for different PFRs sensors and speed requirements.

We note that the OV based models are suitable for the PFR control, as they accommodate reverse movements and have sufficient flexible parameters to be calibrated based on PFR applications.

3.7 Full velocity difference model

To control the values of acceleration and deceleration more smoothly, the full velocity difference model (FVDM) is proposed based on OVM (Jiang *et al.*, 2001) and the governing equation is:

$$a_n(t) = \kappa\left[V(\Delta x(t-\Delta t)) - v_n(t-\Delta t)\right] + \lambda\,\Theta\left(\Delta v_n(t-\Delta t)\right) \\ \Delta v_n(t-\Delta t) + \beta\,\Theta\left(-\Delta v_n(t-\Delta t)\right)\Delta v_n(t-\Delta t) \tag{7}$$

where the Θ is the Heaviside function, κ is a sensitivity constant, λ is the sensitive constant for acceleration and β is the sensitive constant for deceleration. It is noteworthy that the first part of equation (7) is OVM, the second and third parts of equations (7) are modifications for acceleration and deceleration, respectively.

We note that the FVDM inherits most features and advantages of OVM and is suitable for the PFR control for the same reasons as OVM. It is worth noting that the equation (7) simplified to the OVM governing equation (5) when the λ and β are 0. To study conveniently, the OVM model and FVDM

model will be considered as OVM/FVDM model in the following part.

3.8 Intelligent driver model

The intelligent driver model (IDM) (Treiber *et al.*, 2000) has been applied in traffic simulation and wildly used for the ACC control of production vehicles. The governing model is:

$$a_n(t) = \alpha\left[1 - \left(\frac{v_n(t-\Delta t)}{v_0}\right)^{\delta} - \left(\frac{s_0 + v_n(t-\Delta t)\beta + \frac{v_{n(t-\Delta t)}dv}{2\sqrt{\alpha b_n}}}{\Delta x(t-\Delta t)}\right)\right] \tag{8}$$

where v_0 is the desired speed in the free flow, s_0 is the vehicle-vehicle clearance in stand-still situations, β is the minimum steady-state time gap, α is the subject vehicle's maximum acceleration, b_n is the subject vehicle's desired deceleration, δ is free acceleration exponent (i.e. taking a value of 4).

The first two terms of equation (8), $\alpha\left[1 - \left(\frac{v_n}{v_0}\right)^4\right]$, describe the subject vehicle's behavior in the free flow. The last component of equation (8), $\alpha\left(\frac{s_0 + v_n\beta + \frac{v_n dv}{2\sqrt{\alpha b_n}}}{\Delta x}\right)$ describes the deceleration caused by the lead vehicle. Note that these terms are not compatible to negative speed due to the power and square-root operators. Thus, the IDM violates the feature specified in Section 2.1.

3.9 Adaptive cruise control and cooperative adaptive cruise control models

Adaptive cruise control (ACC) and cooperative ACC (CACC) models were developed for automated vehicle control, while the latter considers additional vehicle-to-vehicle communications. Well-known ACC and CACC control models developed by PATH (Milanés and Shladover, 2014) are shown in equations (9) and (10).

The ACC governing equation is:

$$a_n(t) = k_1\left(\Delta x(t-\Delta t) - v_n(t-\Delta t)\Delta t\right) + k_2\Delta v_n(t-\Delta t) \tag{9}$$

where k_1 and k_2 are the sensitive coefficients for the following gap and the speed difference, respectively.

The CACC governing equation is:

$$v_n(t) = v_{n-1}(t-\Delta t) + k_p e_n + k_d e_n \tag{10}$$

where $e_n = \Delta x(t-\Delta t) - v_n(t-\Delta t)\Delta t$, k_p and k_d are sensitive constants for gap and speed difference.

It is worth noting that although equations (10) and (11) are control functions for ACC and CACC, respectively, both of them are linear functions with sensitive constants for gap and speed difference. Mathematically, the control functions for ACC and CACC belong to the linear models with the same form of equation (3) as discussed before.

3.10 Model feasibility analysis results

In conclusion, the nine types of car-following/automated vehicle control models have been analyzed from the aspect of PFR applications. The results are listed in Table 1, and only the OVM/FVDM model and the linear model (including ACC and CACC in PATH) are available to the PFRs.

4. Parameter optimization

The PFRs are different from automated vehicles in their sizes, speeds, purposes and operating environments. As a result, the parameters of car-following models need to be adjusted and optimized to suit RFPs applications. In this section, the topic of parameter optimization is discussed. Section 4.1 introduces the evaluation criterion for evaluating the parameters. Section 4.2 introduces the important inputs $v_{LP}(t)$ and $\varepsilon(t)$ for parameter optimization. Section 4.3 presents the numerical experiments for the linear model and the OVM/FVDM.

4.1 Evaluation criterion

The evaluation criterion for PFRs longitudinal control is a complex study. Many features should be considered in the parameter optimization, such as PFRs' motor capacity and perception devices' measurement range, energy-saving, gap range and LP's using feeling. In this study, the parameter optimization is described as an optimization problem and the objective function is:

$$\min_{C}\left(\alpha G^{\mathrm{A}} + \beta A^{\mathrm{M}} + \gamma A^{\mathrm{A}} + \delta S^{\mathrm{D}}\right) \tag{11}$$

subject to:

$$G^{\mathrm{A}} = \frac{\sum_{0\le m\le M}|g(t_m)|}{M} \tag{12}$$

$$A^{\mathrm{M}} = \max_{0\le m\le M}|a^{\mathrm{PFR}}(t_m)| \tag{13}$$

$$A^{\mathrm{A}} = \frac{\sum_{0\le m\le M}|a^{\mathrm{PFR}}(t_m)|}{M} \tag{14}$$

$$S^{\mathrm{D}} = \frac{\sum_{1\le m\le M}|v^{\mathrm{PFR}}(t_m) - v^{\mathrm{LP}}(t_{m-1})|}{M} \tag{15}$$

$$a^{\mathrm{PFR}}(t_m) = f\left(g(t_{m-1}), v^{\mathrm{g}}(t_{m-1}), v^{\mathrm{PFR}}(t_{m-1}), C\right),\quad \forall m\in[1,M] \tag{16}$$

$$g(t_m) = x^{\mathrm{LP}}(t_m) - x^{\mathrm{FPR}}(t_m) + \varepsilon(t_m),\quad \forall m\in[0,M] \tag{17}$$

$$v^{\mathrm{g}}(t_m) = \frac{g(t_m) - g(t_{m-1})}{\Delta t},\quad \forall m\in[1,M] \tag{18}$$

$$v^{\mathrm{PFR}}(t_m) = v^{\mathrm{PFR}}(t_{m-1}) + a^{\mathrm{PFR}}(t_m)\,\Delta t,\quad \forall m\in[1,M] \tag{19}$$

Table 1 Car-following model feasibility analysis results for PFRs

Model type	Applicable for PFR?	Parameters need to calibrate (if YES)/ Reasons (if NO)
GHR	NO	Violates the feature specified in Section 2.1
Psychophysical model	NO	Violates the feature specified in Section 2.1
Cellular automata model	NO	Discrete results are not working for PFR
CA model	NO	Violates the feature specified in Section 2.1
Linear model/CACC and ACC control functions in PATH	YES	Parameter C_1,C_2,C_3,D_0
OVM/FVDM	YES	$V(s^2)$ and κ,λ, β
IDM	NO	Violates the feature specified in Section 2.1

$$x^{\mathrm{FPR}}(t_m) = x^{\mathrm{FPR}}(t_{m-1}) + v^{\mathrm{FPR}}(t_{m-1})\ \Delta t, \quad \forall m \in [1, M] \tag{20}$$

$$x^{\mathrm{LP}}(t_m) = x^{\mathrm{LP}}(t_{m-1}) + v^{\mathrm{LP}}(t_{m-1})\ \Delta t, \quad \forall m \in [1, M] \tag{21}$$

$$\max_{0\le m\le M}(g(t_m)) - \min_{0\le m\le M}(g(t_m)) < g_{max} \tag{22}$$

$$\max_{0\le m\le M}\left(a^{\mathrm{PFR}}(t_m)\right) \le a_{max} \tag{23}$$

$$M = \frac{T}{\Delta t} \tag{24}$$

where C is the set of parameters to be optimized; T is the operation time for parameter optimization; Δt is PFR's system interval, which is depend on perception devices frequency, computation speed and motor's reaction time; m is an integer; M is the total number of Δt in T; t_m:=$m\Delta t$ is the discrete time at $m\Delta t$; $v^{\mathrm{LP}}(t)$ is a given LP's moving speed for parameter optimization at time t; $x^{\mathrm{LP}}(t)$ is LP's position at time t; $a^{\mathrm{PFR}}(t)$ is PFR's acceleration calculated by person following control model $f(s^2)$, $v^{\mathrm{PFR}}(t)$ is PFR's speed at time t; $x^{\mathrm{PFR}}(t)$ is PFR's position at time t; $g(t)$ is the observed following gap between LP and PFR by PFR's perception devices at time t; $v^{\mathrm{g}}(t)$ is the observed following gap changing speed; $\varepsilon(t)$ is a given LP's periodical and random movements at time t; G^{A} is the mean value of the following gap in T; A^{A} is the mean value of acceleration of the PFR in T; A^{M} is the maximum acceleration/deceleration in T; S^D is the mean value of speed difference between PFR and LP; α, β, γ and δ are the weights of G^A, A^M, A^A *and* S^D; g_{max} is the maximum tolerable gap range for the testing PFR, and g_{max} is limited by the PFR's perception device; a_{max} is the maximum tolerable acceleration of the PFR and a_{max} is depend on PFR's motor capacity and PFR's weight.

Equation (11) is the objective function of parameter optimization, where G^{A} is the mean value of the following gap and a smaller value of G^{A} indicates better performance at corners or in a crowded environment. A^{A} is the average acceleration of the PFR and a smaller value of A^{A} indicates better performance on energy conservation and endurance. A^M is the maximum acceleration/deceleration and a smaller value of A^{M} indicates the following process is smoother and demands less PFR's motor capacity. S^{D} is the speed difference between LP and PFR and a smaller value of S^{D} indicates the PFR can better filter periodical and random movements while maintaining the same speed with the LP. α, β, γ and δ are the weights of G^A, A^M, A^A and S^D. Different requirements of PFR need different values of weights. For example, relatively large values of β and γ (weights of A^M and A^A) are desired for the PFR designed for carrying a large load.

Equations (12)–(15) are the definitions of G^A, A^M, A^A and S^D, equation (16) is the longitudinal control model for PFR. Equation (17) is the definition of the observed following gap between LP and PFR by the PFR's perception devices $g(s^2)$ and the LP's periodical and random movements $\varepsilon(s^2)$ is included. Equations (18)–(21) are the formulas of $v^g(s^2)$, $v^{\mathrm{PFR}}(s^2)$, $x^{\mathrm{PFR}}(s^2)$, $x^{\mathrm{LP}}(s^2)$. Equation (22) is the gap range requirement, which has been discussed in Section 2.2. Threshold g_{max} is determined by the sensors used by PFRs and working scenarios. Equation (23) is the PFR's postulate of the motor power, brake capability of the PFR. As this study investigates PFRs with an electric powertrain (i.e. controlled by the motor's torque), their deceleration and acceleration capabilities are symmetric. Thus, the maximum acceleration and the minimum accelerations are set with same magnitude (or with the same absolute value) a_{max}.

It is worth noting that v^{LP} and ε are important inputs for parameter optimization. They describe the LP's behavior, and their values determine the optimization scenarios for the PFR longitudinal control. The setting of v^{LP} and ε will be discussed in Section 4.2.

4.2 Leading person motion for parameter optimization

The values of v^{LP} and ε for parameter optimization should cover mostly LP's motions. For different person following requirements, the setting of v^{LP} and ε should be adjusted correspondingly. In a slow following speed scenario, such as following elders or individuals with disabilities, the value of v^{LP} should represent a low speed and mild acceleration. And the value of ε should be low frequency. If the PFR is designed to follow adults and children, the value of v^{LP} should accommodate certain drastic motions, such as running and stop-and-go. The value of ε should denote a high frequency with a large amplitude.

The v^{LP} applied in this study covers several representative LP's motions, such as stop, acceleration, deceleration and reverse. The v^{LP} is set to be equation (25). The total length is 120 s, the maximum speed is 3 m/s; five acceleration-deceleration cycles are included; the acceleration magnitude increases from 0.25 to 0.75 m/s^2; the deceleration magnitude increases from −0.25 to −0.75 m/s^2; 30 s with speed is 0 m/s;

16 s with speed is negative. The figure of $v^{LP}(t)$ is shown in Figure 2:

$$v^{LP}(t) = \begin{cases} 0, & 0 \le t < 2 \\ 0.25t - 0.5, & 2 \le t < 6 \\ 1, & 6 \le t < 10 \\ -0.25t + 3.5, & 10 \le t < 16 \\ -0.5, & 16 \le t < 20 \\ 0.25t - 5.5 & 20 \le t < 22 \\ 0.375t - 8.25, & 22 \le t < 26 \\ 1.5, & 26 \le t < 34 \\ -0.375t + 14.25, & 34 \le t < 40 \\ -0.75, & 40 \le t < 44 \\ 0.375t - 17.25 & 44 \le t < 46 \\ 0.5t - 23, & 46 \le t < 50 \\ 2, & 50 \le t < 56 \\ -0.5t + 30, & 56 \le t < 60 \\ 0, & 60 \le t < 70 \\ 0.625t - 43.75, & 70 \le t < 74 \\ 2.5, & 74 \le t < 84 \\ -0.625t + 55, & 84 \le t < 88 \\ 0, & 88 \le t < 98 \\ 0.75t - 73.5, & 98 \le t < 102 \\ 3, & 102 \le t < 108 \\ -0.75t + 84 & 108 \le t < 112 \\ 0, & 112 \le t \le 120 \end{cases} \quad (25)$$

In this study, $\varepsilon(t)$ is set to be 0.03 *sin* $(t\pi)$. The frequency is 0.5 Hz and the amplitude is 3 cm. The $\varepsilon(t)$ is designed to simulate the LP's body periodical movements during walking.

4.3 Numerical experiments and results

A MATLAB program is coded for parameter optimization. Different following models and parameters are applied in this program. The g_{max} and a_{max} values are set as *0.5* m *and* 2 m/s^2, respectively. Δt is set as 0.1 s. The α, β, γ and δ values in equation (11) are set as 1,1,1 and 10, respectively.

4.3.1 Linear model

The linear model governing equations are equations (3)–(4). In the numerical experiments, the value of C_1 is confined between 0 and 20 with an incremental interval of 1; C_2 is confined between 0 and 200 with an incremental interval of 3, C_3 is confined between 0.05 and 0.15 with an incremental interval of 0.05. Therefore, 4158 (21 × 66 × 3) sets of C_1, C_2 and C_3 values are tested. D_0 is fixed at 0.2 m .

The calculation results of $\alpha G^A + \beta A^M + \gamma G^A + \delta S^D$ in equation (11) for each set of parameters are shown in Figure 3. The *y*-axis shows the value of parameter C_1; *x*-axis shows the value of parameter C_2; the upper figure in Figure 3 shows the results with C_3 =0.05, the middle figure with C_3 = 0.1 and the lower figure with C_3 = 0.15. The sets of parameters not satisfying equations (22)–(23) are eliminated (the white part in Figure 3). The minimum value of $\alpha G^A + \beta A^M + \gamma A^A + \delta S^D$ is 2.2233, as marked with a white rectangle at C_1 = 12, C_2 = 3 and C_3 = 0.05 in Figure 3. With this, {C_1 = 12, C_2 = 3, C_3 = 0.05} is the optimal parameter set we found for the linear model; i.e. the optimal linear model for PFR is shown as:

$$a^{PFR}(t) = 12v^g(t - \Delta t) + 3\big(g(t - \Delta t) - 0.2 - 0.05v^{PFR}(t)\big) \quad (26)$$

4.3.2 Optimal velocity model/full velocity difference model

Based on the optimal velocity model equation (6) for car-following, the PFR's optimal velocity function $V(g)$ for the parameter optimization is modified as:

$$V(g) = 2.5 + 3\tanh[0.0055(g - 0.15) - 1.57] \quad (27)$$

where the relationship between gap g and optimal velocity V is shown in Figure 4, the optimal speed range is [−0.45, 5.39] to allow for a small negative speed. Note that when g is shorter than 217 mm, the optimal speed value is negative for the requirement of reverse.

The function of OVM/FVDM is shown in equation (7). As PFRs investigated in this study apply an electric powertrain (i.e. acceleration and brake both controlled by the motor's torque), the acceleration and deceleration processes of a PFR are symmetric. Thus, the parameters of λ and β in equation (7) are set to be equal for the PFR control.

In the numerical experiments, the value of κ is confined between 0.5 and 24 with an incremental interval of 0.5; and λ is confined between −20 and 20 with an incremental interval of 1. As a result, 1968 (48 × 41) sets of parameters of κ and λ values are tested.

The calculation result of $\alpha G^A + \beta A^M + \gamma A^A + \delta S^D$ in equation (11) for each set of parameters are shown in Figure 5. The *x*-axis shows the value of parameter λ; *y*-axis shows the value of parameter κ. The sets of parameters not subject to

Figure 2 The LP speed vLP for parameter optimization

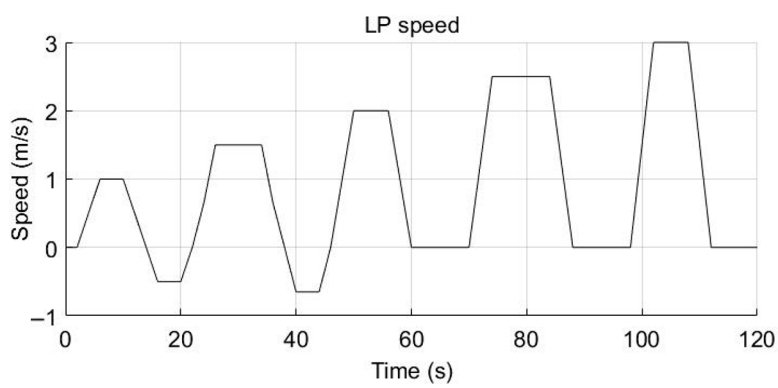

Figure 3 Linear models numerical experiment results

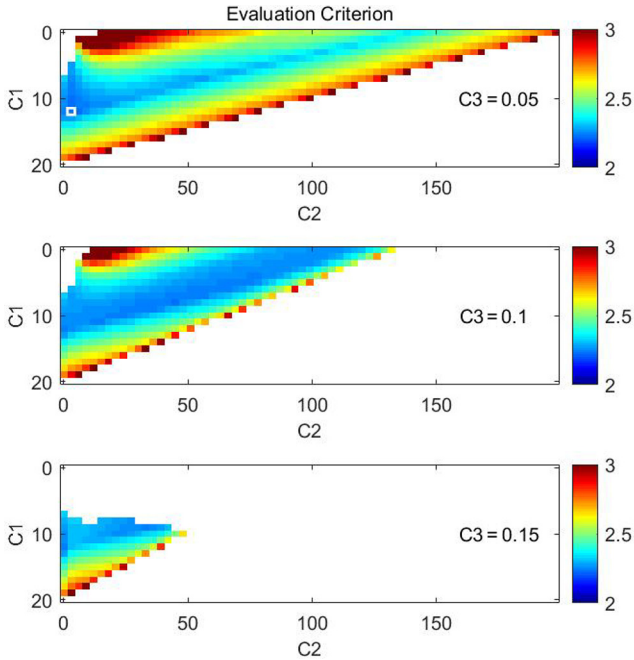

Figure 4 Optimal velocity for PFR

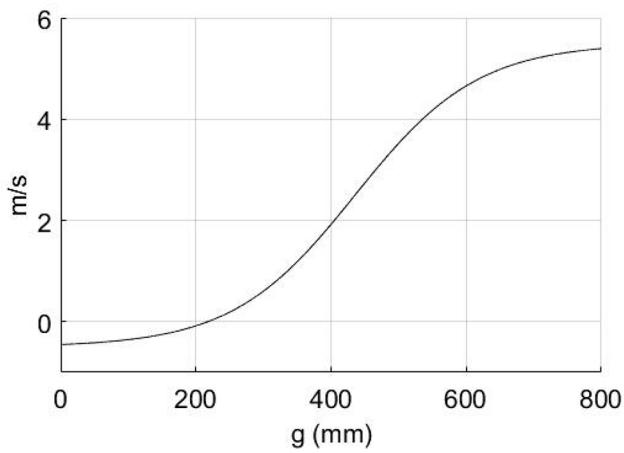

equations (22)–(23) are eliminated (white part in Figure 5). The minimum value is 2.2897, where is marked with a white rectangle at $\kappa = 12$ and $\lambda = 3$ in Figure 5. The parameter set $\kappa = 12$ and $\lambda = 3$ is the result of the parameter optimization for the OVM/FVDM. The optimized function of OVM/FVDM for PFR is shown as:

$$a^{\mathrm{PFR}}(t) = 12\left[V\left(g(t-\Delta t)\right) - v^{\mathrm{PFR}}(t-\Delta t)\right] + 3v^{\mathrm{g}}(t-\Delta t) \tag{28}$$

5. Experiment

A designed PFR with the bar-laser-perception device is developed and tested in the field. The PFR design is introduced

Figure 5 OVM/FVDM numerical experiment results

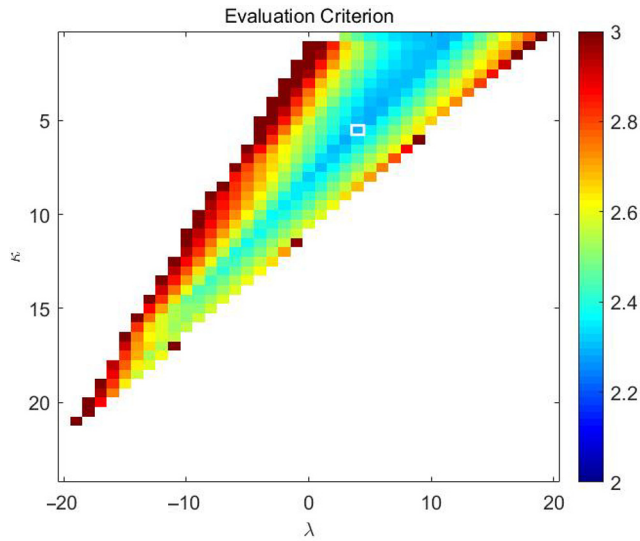

in Section 5.1, and the experiment results are shown in Section 5.2.

5.1 Person-following robot design

As shown in Figure 6, a four wheels PFR is designed. The front two Servo Motor wheels can rotate with different velocities to move and turn. The maximum power is 150 w for each. The motor's real-time speeds are available. The two castor wheels at the rear part support the PFR. The chassis can be simplified as a two-wheeled differential drive model.

The LP perception device has the bar-laser-perception device. As shown in Figure 10, the bar-laser-perception device has two bars, which can move freely through the universal joints. The two bars are connected by a hinge joint. By measuring the distances between the universal joints and plates on both sides, the relative position between PFR and LP can be calculated. The measurement range of the bar-laser-perception-device is 800 mm. The laser range finder type is WT-VL53-485, with ±3% testing error and the maximum measurement frequency is 20 Hz.

The control unit is Arduino Mega 2560, the interface protocols are RS-485 and Modbus. Different car-following models and different parameters can be applied. The calculation frequency is set to 10 Hz. The data from the perception device and motor can be recorded into an SD card.

5.2 Data analysis

Standing, acceleration, deceleration and reverse are tested. Two runs for the linear model and two runs for the OVM/FVDM are recorded. Each record length is about 1 min. The maximum speed is 3.3 m/s. The maximum reverse speed is 1.7 m/s.

The LP's following gap is measured by the bar-laser-perception device. The right and left laser range finder's measurements are noted as dot lines in Figure 7, and the following gaps calculated by the control unit of the PFR are noted as a solid line.

Figure 6 The design of a person-following robot in the experiment: (a) the PFR model; (b) the PFR in the experiment

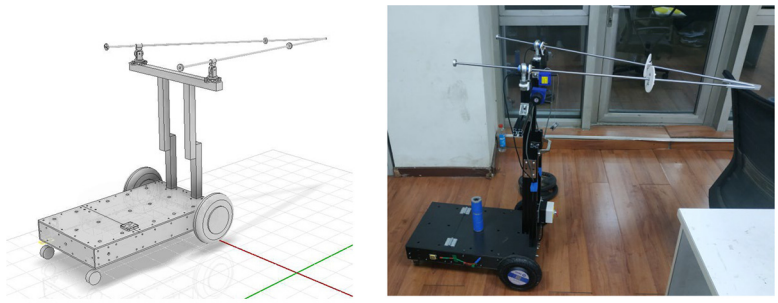

(a) (b)

Figure 7 Gap perception based on the right and left laser range finders' measurements

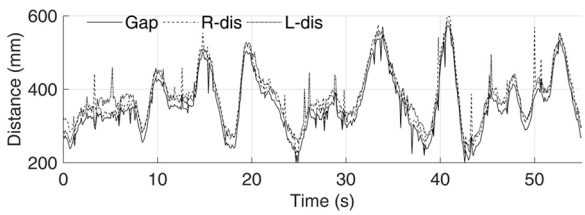

The experiment records are shown in Figure 8, the linear model experiment record is shown in Figure 8(a) and the OVM/FVDM record is shown in Figure 8(b). We see that in the results for both models, the PFR responds to the LP's motions properly and keeps the gap range in 370 mm for the linear model and 330 mm for the OVM/FVDM. Both models can control PFR along the longitudinal direction in normal person-following scenarios.

Compared with the numerical simulation, the field test result acceleration is smaller. This may be caused by the PID setting of the motor controller, and the motors can reach the designed acceleration with a small lag.

6. Conclusion

The studies on the PFR longitudinal control models are insufficient, rarely discussed independently and many longitudinal control exclusive research topics, including the LP's motion features, PFR's following stability and gap range are still deficient. This study supplies a gap in the research on PRFs longitudinal control and provides useful and practical references on PFRs longitudinal control for the related research. The works of this study can be summarized as follows:

- The exclusive features of PFR longitudinal control, including reverse, gap range, no imitation and the LP's periodic/random movement are presented, which are the main goals or requirements for the following study of PFR longitudinal control.
- The knowledge of the car-following/automated driving control model is successfully introduced into person-following studies. Nine widely used car-following models are analyzed from PFRs application, and the linear models and OVM/FVDM models are selected for PFRs.
- The method of parameter optimization for PFRs is presented. In this study, the parameter optimization is described as an optimization problem, and the objective

Figure 8 The following gaps and PFRs speeds of test records: (a) the linear model; (b) the OVM/FVDM

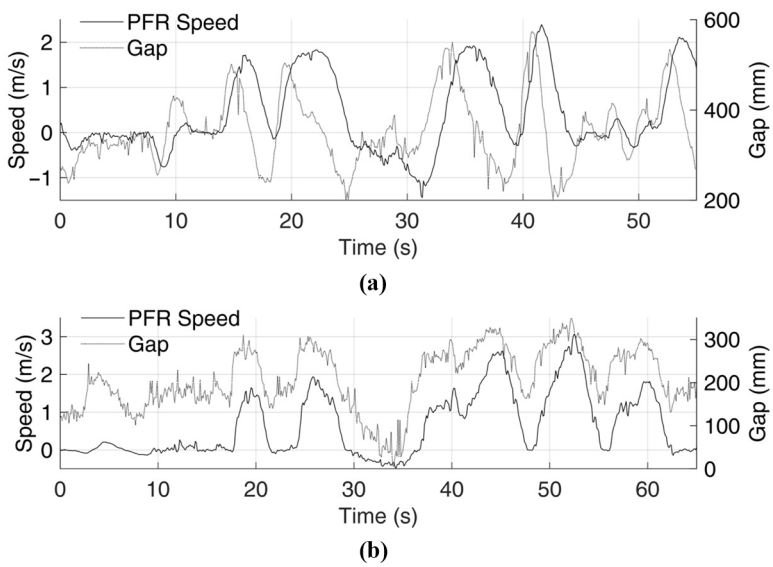

function covers key features of the PFR's longitudinal control, including motor capacity, perception devices' measurement range, energy-saving, gap range and LP's using feeling. The presented parameter optimization method has been successfully applied in the linear model and the OVM/FVDM.

- This study also develops a lab PFR with the bar-laser-perception device for the field tests, and the test results indicate that the proposed longitudinal control models can deal with standing, acceleration, deceleration and reverse in normal person-following scenarios.

There are areas where this paper can be improved in future studies. First, the study of longitudinal control for the PFR will conduct targeted research on different LPs, including child, athlete, adult and elders and even extended the person following robot to the bicycle following robot. Second, the studies of lateral control, obstacle avoidance and routing planning should be integrated into the longitudinal control study to deal with more complex following scenarios.

References

Ahmed, H.U., Huang, Y. and Lu, P. (2021), "A review of car-following models and modeling tools for human and autonomous-ready driving behaviors in micro-simulation", *Smart Cities*, Vol. 4 No. 1, pp. 314-335.

Algabri, R. and Choi, M.T. (2021), "Robust person following under severe indoor illumination changes for mobile robots: online color-based identification update", *21st International Conference on Control, Automation and Systems (ICCAS)*, IEEE, pp. 1000-1005.

Austria, A.C.F., Madolid, M.L.M., Mejia, S.M.D., *et al.* (2021), "Human tracking using size adaptation and vector position for person following robot using MS Kinect Xbox 360", *7th International Conference on Advanced Computing and Communication Systems (ICACCS)*, IEEE, Vol. 1, pp. 1374-1379.

Bae, K., *et al.* (2022), "Component-wise error correction method for UWB-based localization in target-following mobile robot", *Sensors*, Vol. 22 No. 3, p. 1180.

Bando, M., Hasebe, K., Nakayama, A., *et al.* (1995), "Dynamical model of traffic congestion and numerical simulation", *Physical Review E*, Vol. 51 No. 2, p. 1035.

Bao, X.C., Sahdev, R. and Tsotsos, J.K. (2017), "Integrating stereo vision with a CNN tracker for a person-following robot", *International Conference on Computer Vision Systems*.

Brackstone, M. and Mcdonald, M. (1999), "Car-following: a historical review", *Transportation Research Part F: Traffic Psychology and Behaviour*, Vol. 2 No. 4, pp. 181-196.

Cha, D. and Chung, W. (2020), "Human-leg detection in 3D feature space for a person-following mobile robot using 2D LiDARs", *International Journal of Precision Engineering and Manufacturing*, Vol. 21 No. 7, pp. 1299-1307.

Chandler, R.E. and Montroll, H. (1958), "Traffic dynamics: studies in car following", *Operations Research*, Vol. 6 No. 2, pp. 165-184.

Gazis, D.C. and Herman, R. and Potts, B. (1959), "Car-following theory of steady-state traffic flow", *Operations Research*, Vol. 7 No. 4, pp. 499-505.

Gipps, P.G. (1981), "A behavioural car-following model for computer simulation", *Transportation Research Part B: Methodological*, Vol. 15 No. 2, pp. 105-111.

Helly, W. (1959), "Simulations of bottlenecks in single-lane traffic flow", *Theory of Traffic Flow*, pp. 207-238.

Herman, R. and Rothery, R.W. (1965), "Car following and steady state flow", *proc of isttf*.

Islam, M.J., Hong, J. and Sattar, J. (2018), "Person following by autonomous robots: a categorical overview", *The International Journal of Robotics Research*, No. 12.

Jia, S., Wang, L., Wang, S. and Bai, C. (2013), "Fuzzy-based intelligent control strategy for a person following robot", *2013 IEEE International Conference on Robotics and Biomimetics (ROBIO)*.

Jiang, R., Wu, Q. and Zhu, Z. (2001), "Full velocity difference model for a car-following theory", *Physical Review E*, Vol. 64 No. 1, p. 17101.

Kautsar, S., Widiawan, B., Etikasari, B., Anwar, S. and Syai'In, M. (2019), "A simple algorithm for person-following robot control with differential wheeled based on depth camera", *2019 International Conference on Computer Science, Information Technology and Electrical Engineering (ICOMITEE)*.

Lasdon, L.S. Waren, A. Jain, A. *et al.* (1959), "Traffic dynamics: analysis of stability in car Following".

Le, A., Clue, R., Jing, W. and Ahn, I.S. (2018), "Distributed vision-based target tracking control using multiple mobile robots", *IEEE International Conference on Electro/Information Technology*.

Li, L. and Li, X. (2019), "Parsimonious trajectory design of connected automated traffic", *Transportation Research Part B: Methodological*, Vol. 119, pp. 1-21.

Li, X., Xin, W. and Ouyang, Y. (2012), "Prediction and field validation of traffic oscillation propagation under nonlinear car-following laws", *Transportation Research Part B: Methodological*, Vol. 46 No. 3, pp. 409-423.

Michaels, R.M. (1963), "Perceptual factors in car-following", *Proc of Isttf*.

Milanés, V. and Shladover, S.E. (2014), "Modeling cooperative and autonomous adaptive cruise control dynamic responses using experimental data", *Transportation Research Part C: Emerging Technologies*, Vol. 48, pp. 285-300.

Minaeian, S., Jian, L. and Son, Y.J. (2017), "Vision-based target detection and localization via a team of cooperative UAV and UGVs", *IEEE Transactions on Systems, Man and Cybernetics: Systems*, Vol. 46 No. 7, pp. 1005-1016.

Nagel, K. and Schreckenberg, M. (1992), "A cellular automaton model for freeway traffic", *Journal De Physique I*, Vol. 2 No. 12, pp. 2221-2229.

Olatunji, S., Oron-Gilad, T., Sarne-Fleischmann, V., *et al.* (2020), "User-centered feedback design in person-following robots for older adults", *Paladyn, Journal of Behavioral Robotics*, Vol. 11 No. 1, pp. 86-103.

Ozaki, H. (1993), "Reaction and anticipation in the car-following behavior", *Proceedings of International Symposium of Transportation and Traffic Theory*.

Peralta, D., Ramos, M. and Arriola, N.A. (2018), "Person following robotic suitcase", *2018 IEEE 61st International Midwest Symposium on Circuits and Systems (MWSCAS)*.

Ren, Q., Zhao, Q., Qi, H., *et al.* (2016), "Real-time target tracking system for person-following robot", *2016 35th Chinese Control Conference (CCC)*, pp. 6160-6165.

Satake, J. and Miura, J. (2009), "Robust stereo-based person detection and tracking for a person following robot", *Proc IEEE Internat Conf on Robotics and Automation*.

Tarokh M., Merloti P., Duddy J. and Lee M., (Eds) (2008), "Vision based robotic person following under lighting variations", *International Conference on Sensing Technology*.

Treiber, M., Hennecke, A. and Helbing, D. (2000), "Congested traffic states in empirical observations and microscopic simulations", *Physical Review E*, Vol. 62 No. 2, pp. 1805-1824.

Treiterer, J. and Myers, J. (1974), "The hysteresis phenomenon in traffic flow", *Transportation & Traffic Theory*, Vol. 6, pp. 13-38.

Wiedemann, R. (1974), "simulation des strassenverkehrsflusses", Traffic Engineering.

Wu, J., Kulcsár, B., Ahn, S. and Qu, X. (2020), "Emergency vehicle lane pre-clearing: from microscopic cooperation to routing decision making", *Transportation Research Part B: Methodological*, Vol. 141, pp. 223-239.

Wu, J., Ahn, S., Zhou, Y., Liu, P. and Qu, X. (2021b), "The cooperative sorting strategy for connected and automated vehicle platoons", *Transportation Research Part C: Emerging Technologies*, Vol. 123, p. 102986.

Wu, C., Tao, B., Wu, H., Gong, Z. and Yin, Z. (2021a), "A UHF RFID-based dynamic object following method for a mobile robot using phase difference information", *IEEE Transactions on Instrumentation and Measurement*, Vol. 70, pp. 1-11.

Zhang, M., Liu, X., Xu, D., Cao, Z. and Yu, J. (2019), "Vision-based target-following guider for mobile robot", *IEEE Transactions on Industrial Electronics*, Vol. 66 No. 12, pp. 9360-9371.

Further reading

Arem, B.V., Driel, C. and Visser, R. (2006), "The impact of cooperative adaptive cruise control on traffic-flow characteristics", *IEEE Transactions on Intelligent Transportation Systems*, Vol. 7 No. 4, pp. 429-436.

Helbing, D. and Tilch, B. (1998), "Generalized force model of traffic dynamics", *Physical Review E*, Vol. 58 No. 1, pp. 133-138.

Shi, X. and Li, X. (2021), "Empirical study on car following characteristics of commercial automated vehicles with different headway settings", *Transportation Research Part C: Emerging Technologies*, Vol. 128.

Zhou, M., Qu, X. and Li, X. (2017), "A recurrent neural network based microscopic car following model to predict traffic oscillation", *Transportation Research Part C: Emerging Technologies*, Vol. 84, pp. 245-264.

Zhou, M., Yu, Y. and Qu, X. (2019), "Development of an efficient driving strategy for connected and automated vehicles at signalized intersections: a reinforcement learning approach", *IEEE Transactions on Intelligent Transportation Systems*, Vol. 21 No. 1, pp. 1-11.

Corresponding author

Xiaopeng Li can be contacted at: xiaopengli@usf.edu